Mach-Zehnder Interferometer for In-Situ Non-Contact Temperature Monitoring During Thermal Processing of an Optical Fibre

Clarissa M. Harvey, Korbinian Mühlberger, and Michael Fokine

***Abstract*—A Mach-Zehnder interferometer is formed in the transverse plane of an optical fibre. This is exploited to monitor the temperature of any given optical fibre in real time, without any predesigned temperature sensing elements engineered into the fibre and without a need to access the fibre ends. The interferometer is formed by the refraction at the air-glass interface and the subsequent internal reflections within the fibre. The temperature response of the fibre is then measured by quadrature phase shift detection of the interference pattern. For context, this is compared to finite element modelling and a previously studied Fabry-Pérot interferometer configuration. The temperature of an optical fibre was measured from room temperature up to 1174 °C with an error of $\pm 2.6\%$ for the Mach-Zehnder type interferometer. The measurement techniques presented offer a useful tool for precise temperature measurement for applications such as fibre post-processing.**

***Index Terms*—Optical fiber measurements, temperature measurement, laser materials-processing applications, interferometry.**

I. Introduction

OPTICAL fibres have long been an invaluable tool to measure temperature themselves [1], for example, with fibre Bragg gratings [2], [3]. These fibres are specifically designed to be temperature sensors; however, it is also of interest to measure the temperature of an optical fibre that is not designed to be a sensor. For instance, monitoring the temperature of a fibre that is part of another device or is undergoing a thermal post-processing procedure such as splicing [4]–[6] or annealing [7]. Remote temperature sensing can be done using IR cameras or pyrometers for example, but these have limitations in precision and accuracy, particularly, for small, reflective or transparent objects such as optical fibres. These techniques are also based on surface temperature only and require exact knowledge of the temperature-dependent emissivity of the material to be precise.

The interferometric techniques discussed here are practical methods of remotely monitoring the temperature inside an optical fibre without disturbing it or accessing the ends of the fibre. Furthermore, these techniques can be utilised with only prior knowledge of the sample diameter and probe wavelength.

Previous work has been conducted to interferometrically measure the temperature of an optical fibre in real-time by probing the transverse plane of the fibre with a coherent laser source [8]. The reflections from the fibre surfaces then form an optical cavity. The optical path length (OPL) of such a cavity is then dependent on the thermal expansion of the material and the temperature-dependent index change. The phase shift of such an interferometer can be measured using two photo-diodes placed in quadrature in the interference pattern formed. So far this work has primarily focused on a Fabry-Pérot interferometer (FPI) configuration. However, this is only one of multiple possible interferometer configurations within the transverse plane of an optical fibre.

Here, we introduce a Mach-Zehnder interferometer (MZI) configuration as a method of remotely measuring the temperature of an optical fibre. The MZI configuration measures the temperature in a triangular path within the fibre cladding while the FPI configuration measures directly through the fibre core. The advantage of the MZI configuration is that it allows for temperature measurement in optical fibres where the core material is opaque at the probe wavelength or where the index step is high enough to induce additional and detrimental reflections in the FPI.

To experimentally verify that the MZI gives the correct temperature response for a given sample geometry, the MZI was assessed in conjunction with a high-temperature fibre Bragg grating. Namely, a chemical composition grating (CCG) [9] which is alternatively known as a thermally regenerated grating. The measurement of the temperature response of the CCG itself was conducted to be a benchmark for the interferometer techniques explored. The temperature of the fibre was evaluated simultaneously with the previously used FPI configuration to provide a direct comparison between the two techniques. Additionally, it is compared to numerical simulations of the system using finite element modelling (FEM).

II. Experimental Method

A. Interferometer Configurations

The optical paths of both the MZI and FPI configurations are shown in Fig. 1. The MZI is formed when the probe beam is incident on the side of an optical fibre at a glancing angle. The

Manuscript received June 11, 2021; revised July 21, 2021; accepted August 28, 2021. Date of publication September 3, 2021; date of current version November 16, 2021. This work was funded by the Swedish Foundation for Strategic Research under Grant RMA15-0135. *(Corresponding author: Clarissa Harvey.)*

The authors are with the Department of Applied Physics, Royal Institute of Technology, Roslagstullsbacken 21, 114 21 Stockholm, Sweden (e-mail: charvey@kth.se).

Color versions of one or more figures in this article are available at https://doi.org/10.1109/JLT.2021.3109462.

Digital Object Identifier 10.1109/JLT.2021.3109462

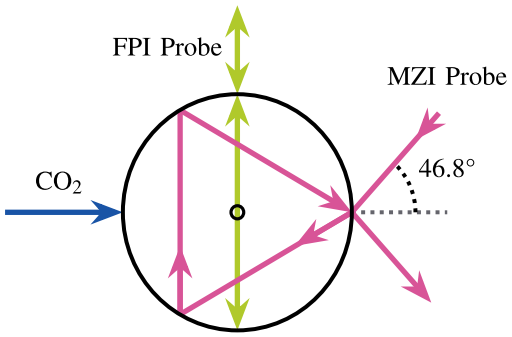

Fig. 1. Diagram of the optical paths of the FPI and the MZI through the transverse cross-section of a circular optical fibre. The FPI is used to measure the average temperature across the fibre diameter and the MZI is used to measure the average temperature of a triangular path through the fibre cladding. The fibre was heated by a CO_2 laser incident on the side of the fibre.

probe beam is split as part of the light is reflected at the surface and the refracted part enters the fibre. The reference path of the MZI is the external reflection from the surface of the fibre. The light that entered the fibre is internally reflected from the surfaces of the fibre and forms the probe arm of the interferometer before leaving the fibre. At a cavity-specific incidence angle, the first external reflection and the second order internal reflections align to form a coincident beam and interfere. In the case of a circular silica fibre with a refractive index $n = 1.457$ at a wavelength of 632.8 nm of the probing laser beam, the required incident angle is 46.8°. For a circular fibre, the established MZI path length is given by

$$L_{\mathrm{MZ}} = k_{\mathrm{MZ}} d = \frac{3\sqrt{3}}{2} d, \tag{1}$$

where k_{MZ} is the MZI path length scale factor and d is the cavity diameter. For a slightly elliptical cavity, the incidence angle changes as well as the OPL of the probe arm (see Appendix A for details).

The other configuration discussed here is the Fabry-Pérot type interferometer. The incident beam is normal to the front surface of the fibre. The partial reflection from the front surface is the reference beam. The rest of the light entering the fibre, the probe beam, is partly reflected again at the back surface of the fibre and then coincides with the reference beam. This configuration relies on the core material having a negligible impact on the probe beam through the fibre. The FPI path length is given by $L_{\mathrm{FP}} = 2\,d$, where d is the fibre diameter.

B. Quadrature Phase-Shift Detection

The OPL of the probe beam changes with the temperature of the fibre. As the OPL changes, the phase difference between probe beam and reference beam changes as well. This has an impact on the intensity response functions of the two interferometers. This means that by monitoring the intensity response function, the temperature-dependent phase change can be measured. For the MZI the intensity response function of the obtained interference pattern can be approximated by

$$I(\phi) = A + B\cos(2\phi), \tag{2}$$

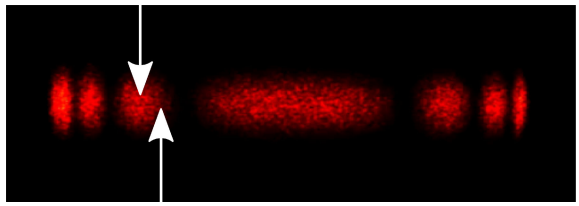

Fig. 2. Photograph of a typically obtained interference pattern with arrows indicating the detector position.

where $A = 0.048 \cdot I_0$ and $B = 0.019 \cdot I_0$ are fitting parameters (the derivation of the fit is given in Appendix B.), I_0 is the initial laser beam intensity and ϕ is the phase shift of the probe beam compared to the reference beam. Further, it has been shown in Ref. [8] that the intensity response function of the FPI can be approximated by 2 as well. In this case, $A = B = I_0$, where I_0 is the intensity of the initial laser beam. This implies that the phase change of both interferometers can be measured by quadrature phase shift detection (as explained in Ref. [10]). To detect the phase shift, two detectors were placed in quadrature within the interference pattern as shown in Fig. 2.

C. Measurement Setup

The experimental system used here consisted of four parts as shown schematically in Fig. 3: the CO_2-laser-based fibre heating system; a Bragg grating temperature measurement system; the FPI configuration and the MZI configuration; It is of note that the Bragg grating is not a necessary part of the interferometric temperature measurement systems but was used here for calibration of the two interferometer configurations.

The fibre heating system used a focused and shuttered CO_2-laser (*Synrad Firestar ti100HS*) operating at 10.6 μm. The CO_2-laser beam spot incident on the fibre had a $1/e^2$-diameter of ≈ 5 mm.

The Bragg grating measurement system consisted of a CCG with a length of 1 mm. The grating was fabricated as described in Ref. [11]. The Bragg wavelength shift of the CCG was monitored in reflection using a white-light source (*Koheras SuperK*) combined with a circulator and an optical spectrum analyser (*BaySpec FBGA-IRS*). The vertical position of the CCG was aligned to be at the centre of the CO_2-laser beam. This was done by aligning for the maximum Bragg wavelength shift and a minimal chirp of the reflected signal ensuring a minimal temperature gradient across the grating.

The temperature was then simultaneously probed using two independent interferometer configurations, each aligned to the same vertical position on the fibre as the heating beam. The Mach-Zehnder interferometer system used a focused HeNe-laser operating at a wavelength of $\lambda_{\mathrm{MZ}} = 632.8$ nm as shown in Fig. 3. The intensity response function of the MZI was measured using two photodiodes S_1 and S_2. The sensors were positioned with a quadrature phase difference in the interference pattern (see Fig. 2) to monitor the full quadrature phase shift.

The Fabry-Pérot interferometer system used a focused solid-state laser operating at a wavelength of $\lambda_{\mathrm{FP}} = 532.0$ nm. The interference pattern was picked off by the PBS and detected

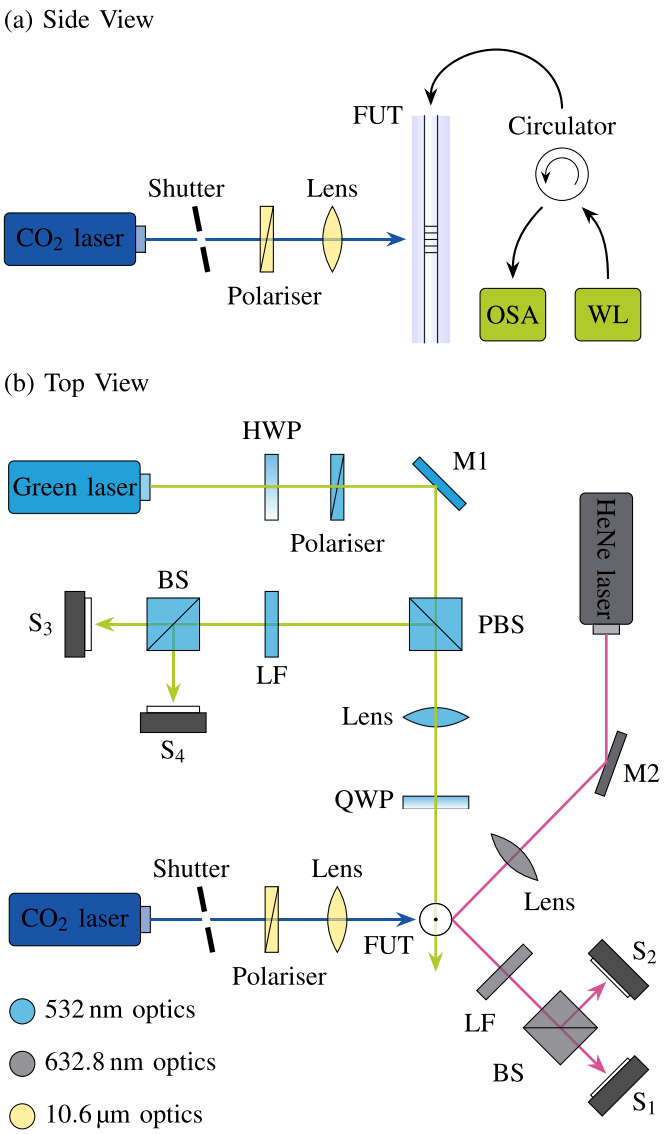

Fig. 3. Schematic of the experimental layout. (a) The White-light source (WL) and optical spectrum analyser (OSA) monitoring the Bragg wavelength of the grating inscribed in the fibre when exposed to a CO_2-laser beam. (b) The CO_2-laser used to heat the fibre was vertically polarised and focused by a ZnSe lens. The MZI system used a HeNe-laser focused on the fibre under test (FUT). The MZI signal was then detected on S_1 and S_2. The FPI system consisted of polarisation and intensity control of the Green laser by half waveplate (HWP) and polariser; M1 beam steering mirror; Quarter waveplate (QWP) and polarising beamsplitter (PBS) ensuring only reflections from the fibre are incident on detectors S_3 and S_4. Line filters (LF) were used to ensure no cross-talk between the interferometer systems. Note that the FUT is the same in (a) and (b).

at the photodiodes S_3 and S_4, which were again placed in quadrature. The distinct probe wavelengths and the use of line filters eliminated cross-talk between the interferometer signals.

D. Calibration Using CCG

The CCG was used as a temperature sensor to calibrate the interferometers to the thermal responses in the fibre. Therefore, the temperature-dependent Bragg wavelength shift of the CCG had to be calibrated first. The grating was sleeved using a fused silica tube and carefully placed adjacent to a K-type thermocouple

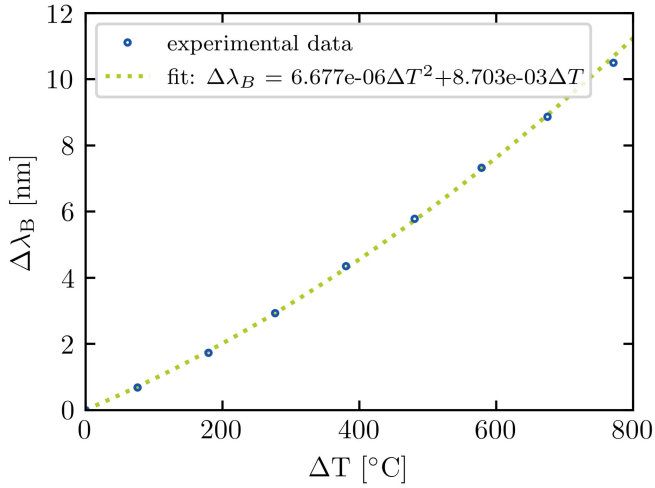

Fig. 4. Calibration of the CCG by monitoring its Bragg wavelength shift while heated in an oven.

inside an oven (*Carbolite CWF 1100*). Both the thermocouple and the sleeved grating were placed in a ceramic tube to reduce temperature fluctuations with increased thermal mass. The ceramic tube was mounted horizontally in the oven. The oven was then heated up to 1000 °C in steps of 100 °C. For each set temperature, the oven was allowed to stabilise sufficiently before the temperature reading of the K-type thermocouple and the Bragg wavelength shift of the CCG were recorded.

The obtained data, shown in Fig. 4 was fitted by the second order polynomial

$$\Delta\lambda_B = 6.677 \cdot 10^{-6}\Delta T^2 + 8.703 \cdot 10^{-3}\Delta T, \qquad (3)$$

with an R^2-value of 0.9995. The root mean square error (RMSE) is ± 74 pm corresponding to ± 8.5 °C comparable to the specified temperature accuracy of ± 7.5 °C of a K-type thermocouple at 1000 °C.

III. Results

The fibre under test (FUT) was heated for a duration of 3 s at 13 different laser power settings between 5.8 W and 26.5 W. An external trigger opened the shutter of the CO_2-laser and simultaneously started the data acquisition of the two interferometers as well as the monitoring of the CCG. Both interferometers and the OSA were set to sample at a frequency of 1 kHz.

A. Mach–zehnder Interferometer: Temperature Measurement in the Fibre Cladding

The measured responses upon heating the fibre, both the Bragg wavelength change of the CCG and the phase change of the MZI, were normalised and a typical result is shown in Fig. 5. For clarity reasons, only every 100th data point of the MZI is plotted. As can be seen from the plot, the heating and cooling responses of the CCG and the MZI are in good agreement. The relation between the Bragg wavelength change of the CCG and the phase response of MZI is plotted in Fig. 6 and fitted by the

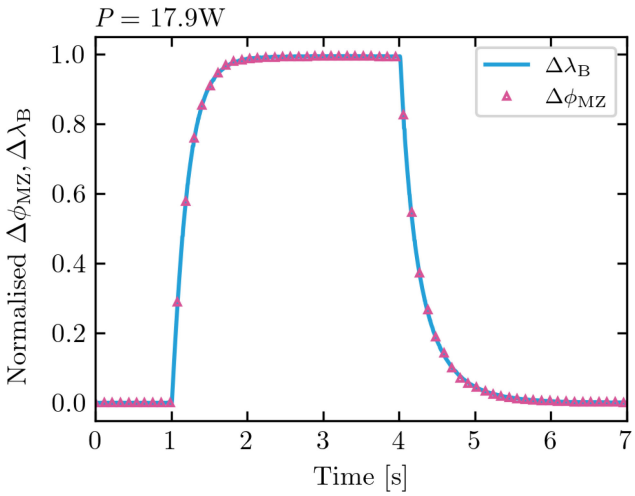

Fig. 5. Comparison of the temperature response of the CCG with the phase change of the MZI.

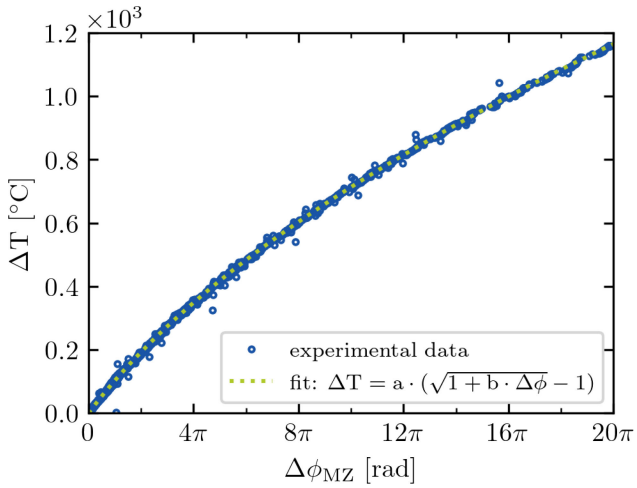

Fig. 7. The calibration curve for the relative temperature change with the phase change in the MZI after calibration with a CCG.

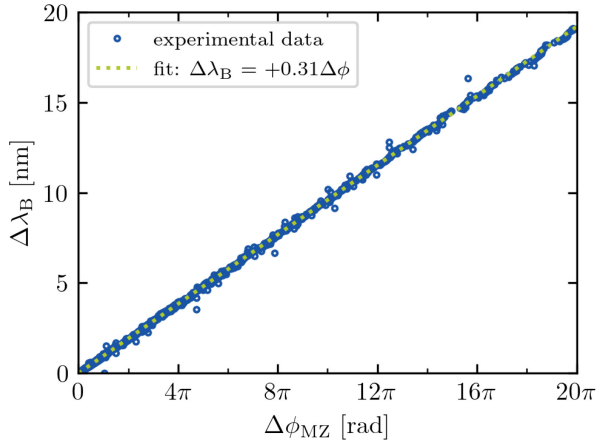

Fig. 6. A plot of the relation of the Bragg wavelength shift of the CCG and the MZI phase change.

linear regression:

$$\Delta\lambda_{\mathrm{B}} = (0.31 \pm 0.04\ \mathrm{nm\ rad^{-1}}) \cdot \Delta\phi. \tag{4}$$

Using 3, the Bragg wavelength change of the CCG can be converted to a temperature change. This enables a final calibration relating the phase change of the MZI to the corresponding temperature change of the fibre core. The result is plotted in Fig. 7. Equating 3 with 4 and solving for ΔT gives the fitting equation:

$$\Delta T = a \cdot \left(\sqrt{1 + b \cdot \Delta\phi} - 1\right). \tag{5}$$

Here, $a = 6.502 \cdot 10^2$ °C, $b = 1.081 \cdot 10^{-1}$ rad^{-1}, the R^2-value is 0.9999 and the RMSE is ±2.987 °C (±0.25%).

B. Fabry-Pérot Interferometer: Temperature Measurement Through the Fibre Core

Analogously to the MZI, the phase response of the FPI has been calibrated to the used CCG. The derived temperature calibration is also given by 5. For the FPI, $a = 6.331 \cdot 10^2$ °C, $b = 1.213 \cdot 10^{-1}$ rad^{-1}, the R^2-value is 0.9999 and the RMSE is ±2.197 °C corresponding to ±0.18%. A detailed description of the evaluation of the FPI can be found in Ref. [8].

C. Comparison of Mach-Zehnder and Fabry-Pérot Interferometer

The thermal response of the fibre was measured using both interferometer configurations and compared to numerical simulations for different power settings of the CO_2-laser. Three example results are shown in Fig. 8. For clarity, only every 100th point of the recorded FPI and MZI data is plotted. The simulations were performed by the finite element method (FEM) in COMSOL. The CO_2-laser beam incident on the 125 μm was set as a Gaussian beam with a $1/e^2$ diameter of 5 mm. The temperature-dependent absorption coefficient of fused silica used was $\alpha(T) = 4\pi(1.82 \cdot 10^{-2} + 10.1 \cdot 10^{-5}\ \mathrm{K^{-1}}(T - 273.15\ \mathrm{K}))/\lambda_{\mathrm{CO_2}}$ with $\lambda_{\mathrm{CO_2}} = 10.6\ \mu$m as reported in Ref. [12]. Convection was evaluated using the COMSOL settings for natural convection on a vertical cylinder. The temperature dependent thermal conductivity, specific heat and emissivity used for the model were obtained from Ref. [13]. The measured and the simulated temperature responses show comparable behaviour. The response upon heating the fibre at a time $t = 1$ s appear to be identical. As the fibre cooled down, after $t = 4$ s, the temperatures measured by the two interferometers were still in good accordance while the simulated fibre cooled down slightly faster. This was attributed to a disparity in the theoretical convection coefficient and the real world airflow conditions around the fibre. An example of the simulated heat distribution in the fibre cross-section is shown in Fig. 9. This simulation corresponds to the highest temperature measured experimentally and the largest thermal gradients that were present in the experiment. The cross-sectional thermal gradient has a steady-state difference of 15 °C from the hottest point on the fibre where the laser is incident on the fibre to the coolest point on the far side. The average temperatures along the respective interferometer paths were ascertained from the simulations and found to only have a difference in measured temperature of 0.5 °C in the hottest and most extreme thermal gradient applicable here.

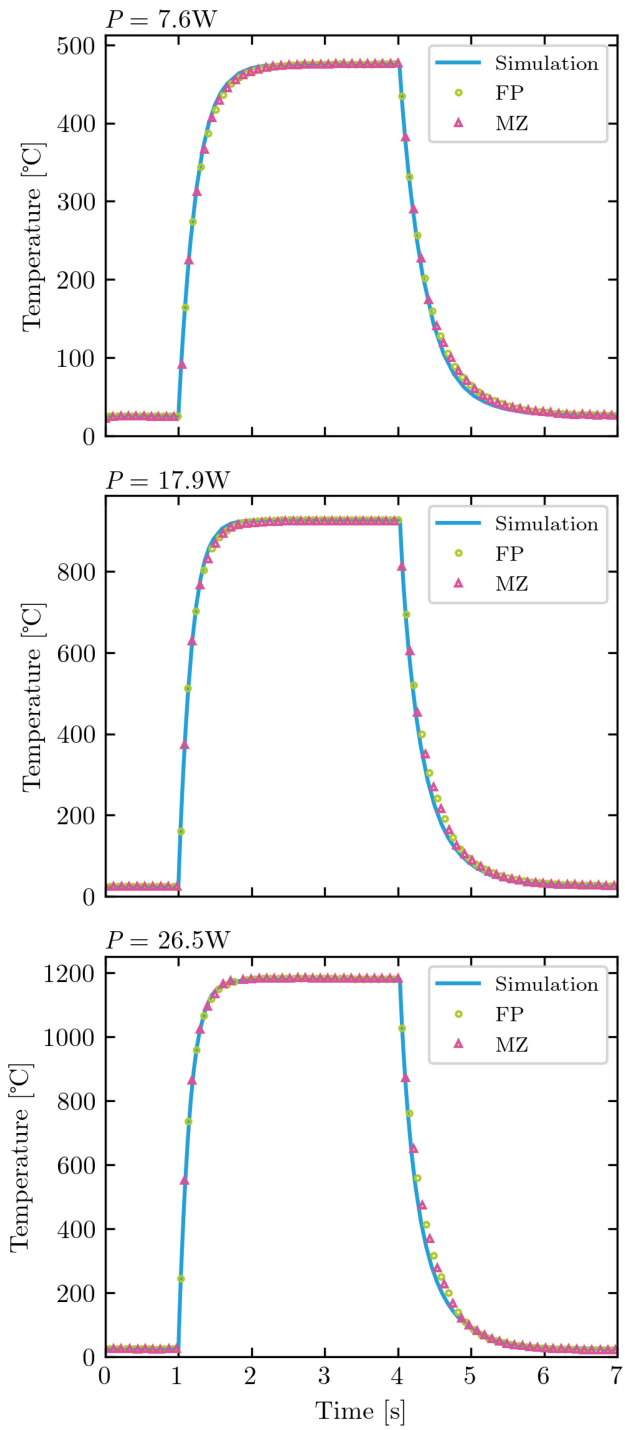

Fig. 8. Example temperature responses of a vertically suspended optical fibre when exposed to a CO_2-laser beam for a duration of 3 s. The data is shown for three different output powers P of the CO_2-laser. The blue line is the corresponding FEM simulation of the system. The pink triangles and green circles show the concurrent temperature response of the MZI and the FPI respectively.

IV. Discussion

The results from the MZI and FPI comparison, Fig. 8, show a strong correlation. The response of each of these interferometer configurations shows an identical temporal response. This indicates that both the MZI and FPI were responding to the same temperature change at the same vertical position in the fibre

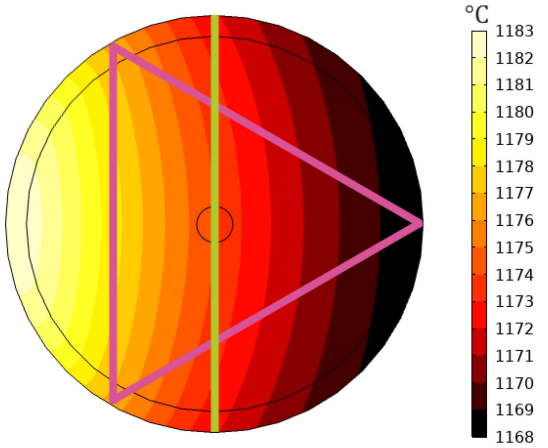

Fig. 9. Simulation of the thermal gradient across the 125 μm diameter fibre cross-section. The plot corresponds to the highest temperature measured ($P = 26.5$ W in Fig. 8) at $t = 4$ s. The average temperature of the cross-section in this simulation was 1173.6 °C. The average temperature along the MZI (pink triangle) and FPI (green line) paths in the simulation were 1173.9 °C and 1173.4 °C respectively. The average core temperature was 1174.2 °C.

with negligible thermal gradients across the transverse plane of the fibre. Thus, these methods of temperature measurements are interchangeable and the most appropriate method can be chosen for a given application.

The phase shift of each interferometer was calibrated using a CCG to give the temperature response of each measurement method. With this calibration, the thermal responses measured by both the FPI and MZI are identical. This demonstrated that there was a negligible effect from the thermal gradients across the fibre as both interferometers exhibited the same heating and cooling curvature. This was corroborated with the simulation results in Fig. 9. The simulation showed that the difference between average temperature in the fibre cross-section, the core temperature and the temperature measured across both the interferometer paths were smaller than 0.8 °C for the most extreme heating case measured in these experiments. This verified that both the average cladding temperature along the MZI path and the core temperature (where the CCG is written) measured comparable temperatures for a sample of this scale.

Since the simulation was in good agreement with the experimentally found values and there was a negligible difference in the temperature measured in different parts of the fibre cross-section, a 125 μm fibre could be viewed as one-dimensional in terms of thermal response. This is in agreement with the assumption made in previous fibre heating models [14], [15]. For larger sample diameters, the thermal response in the centre and cladding is expected to deviate as thermal gradients become more significant.

A useful entity to compare the two interferometers are the relative phase changes in the two configurations. It has been shown in Ref. [8] that the phase change in the FPI configuration, $\Delta\phi$, is related to the Bragg wavelength change through

$$\Delta\phi = \frac{2\pi n_0 L}{\lambda_0 \lambda_i} \cdot \Delta\lambda_{\mathrm{B}}, \tag{6}$$

where λ_0 is the Bragg wavelength of the CCG at room temperature (RT), n_0 is the refractive index of fused silica at RT for the

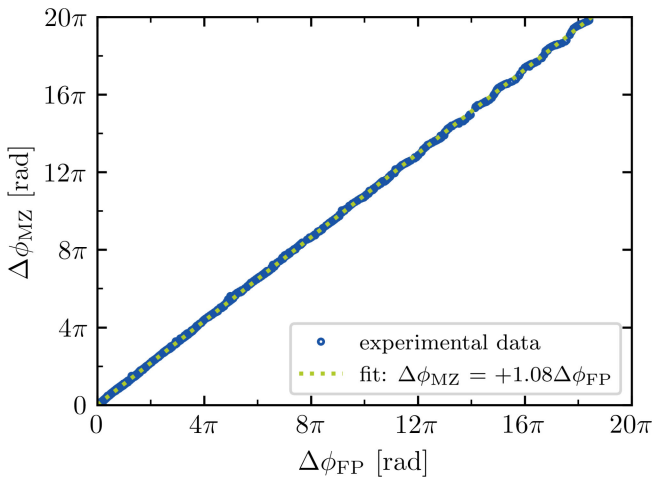

Fig. 10. The experimentally measured relation of the MZI phase change to the phase change in the FPI in the cross-section of a silica optical fibre during heating and cooling.

probing wavelength λ_i, and L is the effective length of the cavity. This relation holds for the MZI as well; providing a simple means to apply the found calibration of phase change to temperature change to different sample sizes or probe wavelengths in either interferometer configuration. Combining 6 for the FPI and the MZI leads to an equation describing the phase change relation of the FPI and the MZI:

$$\Delta\phi_{MZ} = \frac{n_{\mathrm{MZ}}}{n_{\mathrm{FP}}} \cdot \frac{L_{\mathrm{MZ}}}{L_{\mathrm{FP}}} \cdot \frac{\lambda_{\mathrm{FP}}}{\lambda_{\mathrm{MZ}}} \cdot \Delta\phi_{\mathrm{FP}}, \tag{7}$$

where $n_{\mathrm{FP}} = 1.461$ is the refractive index of silica at $\lambda_{\mathrm{FP}} = 532.0$ nm, $L_{\mathrm{FP}} = 2 \cdot d$ is the cavity length of the FPI, $n_{\mathrm{MZ}} = 1.457$ is the refractive index at $\lambda_{\mathrm{MZ}} = 632.8$ nm and $L_{\mathrm{MZ}} = k_{\mathrm{MZ}} \cdot d$ is the cavity length of the MZI, k_{MZ} is the MZI path length scale factor and $d = 125$ μm is the fibre diameter. The experimentally found relation between the two phase changes is plotted in Fig. 10 and fitted by the linear regression

$$\Delta\phi_{\mathrm{MZ}} = (1.08 \pm 0.09) \cdot \Delta\phi_{\mathrm{FP}}, \tag{8}$$

which is in good agreement with the theoretically expected value 1.09 for a circular fibre. Using the experimentally found value of 1.08, the MZI scale factor is deduced to be $k_{\mathrm{MZ}} = 2.566$ which corresponds to a fibre eccentricity of 0.975 (see Appendix A for details). The cross-section of the fibre was examined under a microscope (*Nikon Eclipse LV100*) and the measured eccentricity was 0.980 ± 0.005.

The FPI has previously been shown to work as a non-contact temperature sensor for an optical fibre [8]. Nonetheless, there are limitations to this configuration imposed by the core material of the fibre. If the core has a high index contrast, then multiple FPI signals form and complicate the measurement. Additionally, if the core is of a material that is opaque to the probe wavelength, this blocks the optical path of the FPI. The advantage of the FPI configuration is that it is relatively robust to fibre alignment and subsequent vibration or movement.

The MZI has been shown to be a viable means of measuring the core temperature by monitoring the OPL in the cladding at a specific point on an optical fibre. This interferometer configuration functions even if the core material is opaque at the probe beam wavelength. However, the MZI configuration is more sensitive to slight misalignment and the error in the recorded temperature-change increases for more elliptical or misaligned fibres than it does for the FPI configuration due to the longer optical path. The reason is that the measured temperature change is obtained from the OPL and the latter can noticeably vary from the OPL of a perfect circle for eccentricities of even a few percent. A more detailed discussion of this effect is reviewed in Appendix A. However, the ellipticity of the fibre can be compensated for by having a priori knowledge of the exact fibre geometry and orientation. This is a limitation of the MZI and leads to a systematic error in the recorded temperature change of up to 1.9% as discussed in Appendix A. In addition to the 0.7% error from the CCG calibration, the temperature measured by the MZI had a systematic offset of 2.6%. Especially compared to the FPI, the MZI was more sensitive to alignment. As a specific probe beam angle is required relative to the fibre surface, the MZI is less robust in respect to the vibration or movement of the fibre being measured. This ideal probe beam angle is also slightly temperature depended as thermo-optics effects change the refractive index of the material. This effect can be seen in the fluctuations at higher temperatures in Fig. 10 as the MZI was aligned to the ideal probe angle at room temperature.

With known calibration values for silica, both interferometers can be scaled for different fibre diameters and different probe wavelengths as described in 7. This allows for the measurement of optical fibres of varying sizes with different probe beam wavelengths but also for the measurement of any circular structure given a known OPL for each configuration.

V. Conclusion

Both Mach-Zehnder and Fabry-Pérot interferometer configurations have been assessed with a CCG for measuring the temperature at a specific point on an optical fibre. The temperature sensing capabilities of the MZI and the FPI have both been verified with respect to each other and match the simulated behaviour. The merits of each configuration have been analysed and verified. The Mach-Zehnder interferometer was used to measure the average temperature along a triangular path in the fibre cladding up to $1174\,^{\circ}\mathrm{C} \pm 31\,^{\circ}\mathrm{C}$. It has been shown that the Mach-Zehnder interferometer configuration is a viable means of remotely measuring the precise temperature of an optical fibre in real-time.

Appendix A
Effect of Sample Ellipticity on Temperature Probing

In a circular fibre, the triangular Mach-Zehnder path length can be calculated using the law of reflection, Snell's law, and geometry. In this case, the path must be an equilateral triangle that has a perimeter of $L_{\mathrm{MZ}} = k_{\mathrm{MZ}} d = 3\sqrt{3}d/2$ where k_{MZ} is the Mach-Zehnder optical path length scale factor and d is the diameter of the fibre sample. In reality, optical fibres have some ellipticity to the cross sectional area. For commercially available fibres, this is typically an eccentricity that varies by $\approx 1\%$ from an ideal circle. The eccentricity can be much higher for speciality

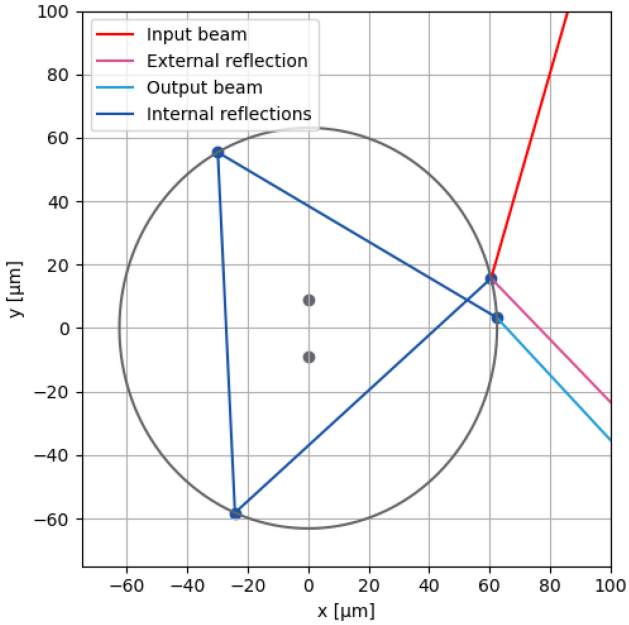

Fig. 11. An optical path through an elliptical fibre cross-section that satisfies the Mach-Zehnder interferometer conditions of having a parallel reference beam and probe beam. The grey dots are the focuses of an ellipse with an eccentricity of 0.99. The point of incidence is rotated 15° from the semi-minor axis of the ellipse. This condition then has a corresponding MZI input angle of 55.6°.

optical fibres drawn in research facilities. This is also an area where thermally post-processed fibres are of particular interest. Thus, it is necessary to know the impact the fibre ellipticity has on the OPL and subsequently on the temperature measurement. Fig. 11 illustrates an example optical path in an elliptical fibre found using geometrical optics. The external reflection and the output signal beam are parallel and produce an interference pattern. Once the criteria for a MZI have been met, the geometrical optics give the path length scale factor $k_{\mathrm{MZ}} = 3\sqrt{3}d/2$. For an elliptical fibre the path length scale factor k'_{MZ} can differ by a few percent. The example fibre depicted in Fig. 11 has an eccentricity of 0.99. In this case, the found OPL is 0.5% shorter than the expected $3\sqrt{3}d/2$. Using 7 and 5 this corresponds to a systematic error in the measured temperature of up to 1.5%. It is of note that at eccentricities higher than $\approx 5\%$, the conditions for the MZI are no longer satisfied as the necessary incident angle lies outside of the Brewster angle for silica. At this point, the largest deviation in OPL is $\approx 2.8\%$ which corresponds to a temperature measurement error upper limit of $\approx 1.9\%$.

The other main caveat of this analysis is that for eccentricities of greater than 1%, the necessary conditions to form a Mach-Zehnder interferometer can only be met when the probe beam is incident on one of the axes of the ellipse. So for more elliptical fibres, greater control of the fibre orientation is required. The MZI optical path length of a fibre with a known ellipticity and orientation can be calculated and the temperature of particularly elliptical samples can be accurately measured. The calculated path length adjustment required for an on-axis probe beam is shown in Fig. 12 and fitted by the linear regression

$$k'_{\mathrm{MZ}}/k_{\mathrm{MZ}} = 0.5 \cdot d_y/d_x + 0.5. \tag{9}$$

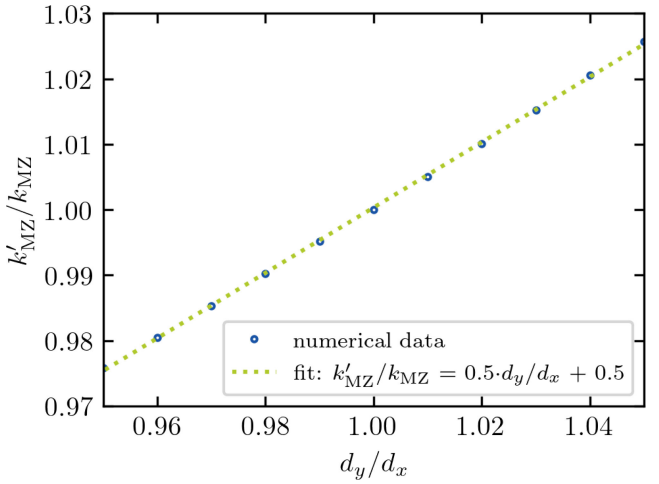

Fig. 12. The adjustment to the MZI optical path length required for a probe beam incident on the axis of an elliptical fibre. Where d_y and d_x are the fibre diameters d, in the y and x directions respectively as is in Fig. 11.

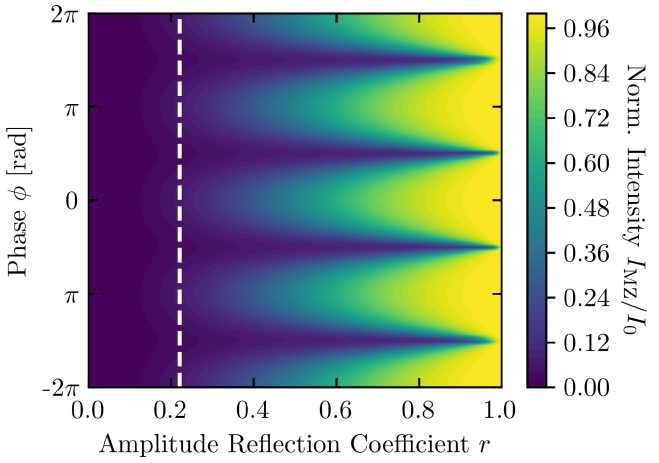

Fig. 13. Intensity response function of the MZI. The dashed line at $r = 0.22$ corresponds to fused silica.

Appendix B
Intensity in the MZI Interference Pattern

The initial probe beam for a Mach-Zehnder type interferometer is assumed to have an amplitude a_0. It is partially reflected by the optical fibre so that the first reflection has an amplitude $a_1 = a_0 \cdot r$, where r is the amplitude reflection coefficient for the air-glass interface. The amplitude of the internally refracted and reflected probe beam is given by

$$a_2 = a_0 t t' r'^2 e^{i\phi} \left(1 + r^3 e^{i\phi} + \left(r^3 e^{i\phi}\right)^2 + \cdots\right), \tag{10}$$

where r' is the amplitude reflection coefficient for the glass-air interface, t and t' are the amplitude transmission coefficients for the air-glass and glass-air interfaces respectively and ϕ is the phase the internal beam gains with each round trip inside the cavity. Using the Stokes relations, it follows that the amplitude of the overlapping probe beam and reference beam is given by

$$a_1 + a_2 = a_0 \cdot r \frac{1 + re^{i\phi}}{1 + r^3 e^{i\phi}}. \tag{11}$$

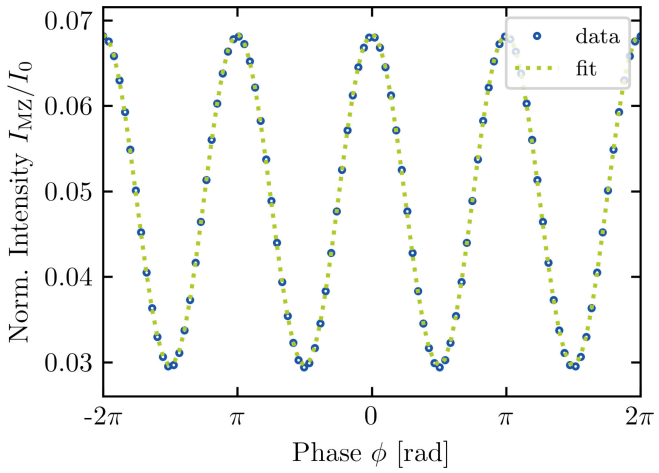

Fig. 14. Slice of the intensity response function of the MZI for $r = 0.22$ with a sinusoidal fit $I_{MZ}/I_0 = A + B \cdot \cos(2\phi)$, where I_0 is the initial laser beam intensity, $A = 0.048$ and $B = 0.019$.

The intensity response function I_{MZ} of the MZI is then described by

$$I_{MZ} = I_0 \cdot \left| \frac{a_1 + a_2}{a_0} \right|^2 = I_0 \cdot r^2 \frac{r^2 + 2r\cos(2\phi) + 1}{r^6 + 2r^3\cos(2\phi) + 1}, \quad (12)$$

where I_0 is the initial laser beam intensity. This intensity response function is plotted in Fig. 13 for r-values $r \in [0, 1]$ and phase values $\phi[\,\mathrm{rad}] \in [-2\pi, 2\pi]$.

For an air-silica interface, the amplitude reflection coefficient is $r = 0.22$. The corresponding slice of the intensity response function is plotted in Fig. 14 and fitted by 2. Here, $A = 0.048$ and $B = 0.019$ and the R^2-value is 0.9999. Given that the R^2-value is approximately 1, for an air-silica interface, the intensity response function can be assumed to have a sinusoidal behaviour.

REFERENCES

[1] E. Udd and W. B. Spillman, *Fiber Optic Sensors: An Introduction for Engineers and Scientists*, 2nd ed. Hoboken, NJ, USA: Wiley, 2011.
[2] R. Kashyap, *Fiber Bragg Gratings*. San Diego, CA, USA: Elsevier, 2010.
[3] A. Othonos, K. Kalli, and G. E. Kohnke, "Fiber Bragg gratings: Fundamentals and applications in telecommunications and sensing," *Phys. Today*, vol. 53, no. 5, pp. 61–62, May 2000.
[4] A. D. Yablon, *Optical Fiber Fusion Splicing* (Ser. Springer Series in Optical Sciences), vol. 103. Berlin/Heidelberg, Germany: Springer-Verlag, 2005.
[5] G. M. Rego, P. V. Marques, J. L. Santos, and H. M. Salgado, "Estimation of the fibre temperature during the inscription of arc-induced long-period gratings," *Opt. Commun.*, vol. 259, no. 2, pp. 620–625, Mar. 2006.
[6] G. Rego, L. M. N. B. F. Santos, and B. Schröder, "Estimation of the fiber temperature during an arc-discharge," *Microw. Opt. Technol. Lett.*, vol. 50, no. 8, pp. 2020–2025, Aug. 2008.
[7] P. Holmberg, F. Laurell, and M. Fokine, "Influence of pre-annealing on the thermal regeneration of fiber Bragg gratings in standard optical fibers," *Opt. Exp.*, vol. 23, no. 21, Oct. 2015, Art. no. 27520.
[8] K. Mühlberger, C. M. Harvey, and M. Fokine, "In-situ non-contact high-temperature measurement of an optical fiber up to the glass softening point," *Opt. Exp.*, vol. 29, no. 5, pp. 7825–7832, 2021.
[9] M. Fokine, "Underlying mechanisms, applications, and limitations of chemical composition gratings in silica based fibers," *J. Non-Crystalline Solids*, vol. 349, pp. 98–104, 2004.
[10] J. Wang and J. L. Pressesky, "Quadrature phase shift interferometer (QPSI) decoding algorithms and error analysis," *Proc. SPIE*, vol. 5188, pp. 71–79, 2003.
[11] M. Fokine, "Growth dynamics of chemical composition gratings in fluorine-doped silica optical fibers," *Opt. Lett.*, vol. 27, no. 22, 2002, Art. no. 1974.
[12] A. D. McLachlan and F. P. Meyer, "Temperature dependence of the extinction coefficient of fused silica for CO_2 laser wavelengths," *Appl. Opt.*, vol. 26, no. 9, p. 1728, May 1987.
[13] A. Grellier, "Characterisation of optical fibre tapering using a CO_2 laser," Ph.D. dissertation, Univ. Kent Cantebury, 2000.
[14] C. Liao, D. Wang, Y. Li, T. Sun, and K. T. V. Grattan, "Temporal thermal response of Type II-IR fiber Bragg gratings," *Appl. Opt.*, vol. 48, no. 16, p. 3001, Jun. 2009.
[15] A. Grellier, N. Zayer, and C. Pannell, "Heat transfer modelling in CO_2 laser processing of optical fibres," *Opt. Commun.*, vol. 152, no. 4-6, pp. 324–328, Jul. 1998.